ARCHAEOLOGY AND MATERIAL SCIENCE: Sacred Stones or Clever Fakes?

Natalie Chen, Zachary Ciappa, Jack Ecklund, Abigail Frey, Lucas Horowitz-Kurtzberg, Darby Ko, Serena Lorenzo, Julianne Ma, Andie Park, Alexica Perez, Luke Shao

Assistants: Ece Onatca and Katelyn Rohlf

Advisor: Dr. Maria Masucci

ABSTRACT

Around the globe, greenstone beads have been found in burial and ritual contexts, suggesting their cultural significance as symbols of wealth and status. Our study analyzed the composition of greenstone beads from suspected production sites in Guangala and Manteño settlements in the southwestern coastal region of Ecuador. Understanding the origin and composition of these beads is essential to understanding the history of pre-Columbian societal structure and cross-cultural trade, as well as the value of greenstone beads in the coastal Guangala and Manteño cultures. In this study, we aim to determine the raw materials used to manufacture the greenstone beads, and determine the location and rarity of the minerals. We performed a multidisciplinary analysis including mineralogical analysis with optical petrography, chemical analyses through a hydrochloric acid test, and Fourier Transform Infrared Spectroscopy with Attenuated Total Reflectance (FT-IR-ATR) examined with Pearson's and Spearman's correlation rank order analysis of the spectra to identify and compare the samples. Through the analyses, we determined that the artifacts were composed of different minerals, predominantly present in local and common rock formations. Our results suggested that the greenstone beads served as an essential domestic export for societies in a greater coastal trade network. Our diverse methodology further provides a novel approach to archaeological research, demonstrating the utility of combining cultural, chemical, geological, and statistical analyses.

INTRODUCTION

Across cultures, the color green is revered and valued for its cultural and material significance. Particularly for the ancient societies of Latin America, greenstones represented power, fertility, and life (Delgado-Robles et al. 2015:3; Piperno 2003). Despite the cultural importance, recovered greenstone artifacts are often hastily classified without analysis by archaeologists as jadeite or nephrite, two minerals that are both commonly referred to as "jade" (Peterson 2010:3; Aguilar-Melo et al., 2019). Greenstone beads found throughout Latin America are often believed to be produced in Ecuador; however, neither jadeite nor nephrite is known to be present there (Shimada 2009). In cases where analyses have been conducted, the greenstone samples of similar phenotypes to "jade" are found to be composed of a wide variety of minerals (Delgado-Robles et al. 2015; Queffelec et al., 2018). Regardless, archaeologists continue to identify greenstone artifacts based on their color and appearance, even after this method was shown to be inaccurate (Peterson 2010). The Guangala and Manteño cultures of coastal Ecuador, spanning 200 B.C.E. to 1540 C.E., have left behind finely-made greenstone beads, which are often assumed to be "jade" (Juengst et al. 2025; Piperno 2003:354-359). As in many studies, this identification was made without any compositional testing (Carter and Helmer 2015:56).

Archaeologists have only recently begun to use modern analytical chemistry techniques to identify the minerals present within samples of greenstone artifacts (Knight et al. 2024; Zhao et al., 2014). Specifically, Fourier Transform Infrared Spectroscopy (FT-IR) has successfully been used as a method to examine the chemical composition of samples, and can help identify the type of greenstone used. Not only is FT-IR an efficient method for identifying chemical composition, but FT-IR using Attenuated Total Reflectance (FT-IR-ATR) is also a non-destructive method, which is essential to analyses of irreplaceable artifacts (Glavcheva et al. 2014). Optical petrography and thin-section mineralogical analysis have become useful methods alongside studies of archaeological chemistry rather than just elemental analysis alone. Petrographic analysis is destructive; however, it remains the preferred method for understanding the nature and composition of geological resources in a region (Masucci and Macfarlane 1997). A holistic understanding of the local geology allows for further research into the production source of ancient artifacts.

Given the success of the application of FT-IR in other regions where greenstone artifacts have been discovered, the current study aims to, for the first time, analyze the chemical and physical properties of greenstone artifacts from coastal Ecuador in order to identify their composition (Delago-Robles et al. 2015). The artifacts include pendants and beads, both complete and in progress, found from bead workshops and surrounding sites (**Figure 1**). We compared artifacts' FT-IR-ATR spectra to databases of chemical FT-IR records. Petrographic analyses of rock and mineral types local to the region were also compared. This study aims to identify the chemical composition of the greenstone beads and determine which raw materials, local or imported, were used for production. This study also aims to correct and clarify the possible inaccurate assessment of greenstone artifacts as "jade." Our project contributes to information on the Guangala and Manteño cultures, and also demonstrates the value of complementary methods typically used solely in the physical and chemical sciences to archaeological studies.

Figure 1: Rock samples and artifacts collected from various locations in southwest Ecuador.

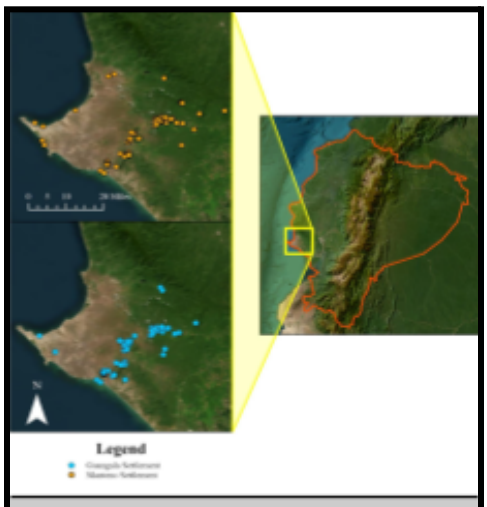

Figure 2: Both Manteño and Guangala settlements were found to have bead-making workshops.

BACKGROUND

Cultural

In our study, we focused on the Guangala and the Manteño cultural phases in southwestern Ecuador. The Guangala were a population native to the modern Guayas and Santa Elena provinces of the southern coastal lowlands of Ecuador. They lived along the coast and the inland plains in numerous dispersed settlements that traded with each other and the surrounding populations (Reitz and Masucci 2004; Masucci 1995:72). Though there is little evidence to indicate the social complexity of Guangala society, the Guangala were skilled craftsmen, specializing in the production of small beads (Masucci 1995). The Manteño, who followed the Guangala, moved from dispersed settlements to more densely concentrated ports along the coastline south of the current-day province of Esmeraldas (Piperno 2008; Reitz and Masucci 2004:11). The Manteño displayed evidence of a hierarchical society with community specialization surrounding occupation that facilitated the production and trade of various goods, including greenstone beads (Reitz and Masucci 2004:31; Cabera 2015; Staller 2001:67-68). Alongside greenstone beads, other artifacts associated with upper-class burials of surrounding cultures, such as obsidian and *Spondylus* shell ornaments, were found in various stages of production at Guangala sites. Quantities found far beyond local consumption suggest that these artifacts were being produced locally for export (Masucci 1995:72; Masucci 2008:500). Archaeologists working in adjacent regions of the Ecuadorian highlands and Peruvian coast cited the Guangala and later Manteño workshops as the source of shell and greenstone beads (**Figure 2**). In excavated workshops, evidence of production using chert drills supports the hypothesis that the greenstone beads of other cultures originated in Ecuador (Gwinnett 1998).

Despite evidence suggesting localized production of greenstone beads, Guangala and Manteño burials rarely contained more than one or two beads, as opposed to hundreds found in burials of the Moche culture in nearby Peru (Staller 2001:76; Shimada 2009:14). This indicates that these items were not as significant to local funerary customs compared to the massive greenstone production scale that the Guangala and Manteño sustained. If the greenstone beads were considered high-value personal items or held ritual significance within Guangala and Manteño society, the beads would have been found in burials at high frequency (Piperno 2003:254). Instead, the scarcity of greenstone in this context supports the interpretation that this region of Ecuador served as a production center. This pattern aligns with broader Andean practices; certain goods functioned more as portable wealth or symbols of regional connectivity than personal items that needed to be kept through death. However, this is just one interpretation of the historical significance of greenstone beads in Ecuadorian society. It is also possible that the value of the greenstone in Ecuadorian society may have lied in its use by individuals rather than in its role within broader economic or political exchange systems (Manrique-Ortega et al. 2014).

Clues to the cultural value of greenstone for Ecuadorian coastal peoples may have also rested in *Spondylus* shells, which can only be obtained by specialist divers, therefore raising the exclusivity and value of the beads. However, there is evidence of *Anadara tuberculosa*, which was easier to collect than the *Spondylus* shell, being used to create imitation beads (Reitz and Masucci 2004; Carter and Helmer 2015). Similarly, in the excavations of royal tomb sites in Guatemala, there were ceramic beads that had been "painted to look like jade" as the "color and

symbolism of jade was so desirable that imitations were created and used," which further support the potential of a similar approach to be used regarding the Ecuadorian greenstone beads (Knight et al. 2024:2). An imitation version of "jade" is one possible answer to the question of the composition of the greenstone beads.

However, it is also important to acknowledge that it may not have been strictly material value that led to the prominence of greenstone beads. The symbolism of the color green itself may have been sufficient to give value to the beads both within Ecuador and in surrounding cultures (Kokaly et al. 2017). The color green held strong symbolism for fertility and health, and was believed to prevent snake bites, epilepsy, dysentery, and other ailments (Boomert 1987). Others have proposed that Manteño societies used greenstone beads as "a primitive form of currency" (Wilbert 1974) based on the presence of strings of beads on a Manteno balsa raft encountered by Spanish sailors off the coast of Ecuador in 1525 (Currie 1995). This cross-cultural "symbolically charged raw material" has created a long-lasting, global appreciation for the stone's beauty and historical value, regardless of the production or reason (Kokaly et al. 2017).

Geological

To fully understand the significance of the greenstone used in the production of the beads, our study aims to understand their composition and, therefore, their source. Whether the greenstone used to produce the beads is readily available locally depends on their relation to the geographical location and geological history of Southwest Ecuador (**Figure 3**) (Aizprua et al. 2020). Ecuador lies upon the subduction of the oceanic Nazca plate beneath the continental South American plate, spurring the formation and continual growth of the Andes. (Witt et al. 2018). This area, concentrated primarily in the coastal lowlands of Southwest Ecuador, is primarily a semiarid region at sea level. The central coastal region primarily consists of rocks from the Basic Igneous Complex, especially volcanic and volcaniclastic. Further south, the region becomes more dominated by younger sedimentary deposits, including sandstones, shales, mudstones, and conglomerates (Masucci and Macfarlane 1997:774).

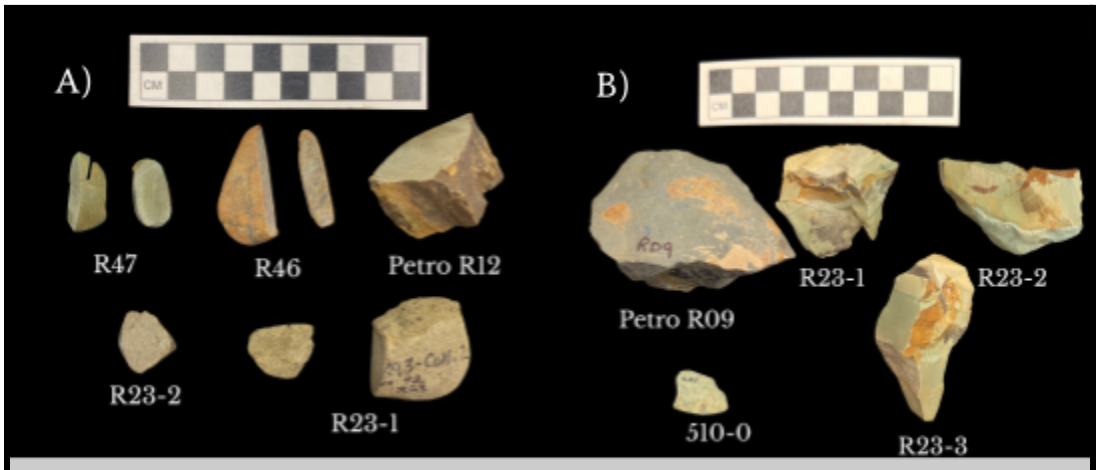

Figure 3: Images of all of our samples taken on a smartphone (A) samples of green rock found from the river beds and surrounding area (B) more samples of green rock

The Chongon-Colonche range, which stems out of the southwestern coastal lowlands, serves as a transition between this semiarid region and the more tropical climate further north (Masucci and Macfarlane 1997:773). Within the Chongon-Colonche range, there are various formations. The Piñon formation, which overlays the coastal regions of southwest Ecuador as an oceanic floor, consists of tholeiitic basaltic and basalt-andesitic lavas. Also within the range is the Cayo formation, a zeolitized deposit following an inactive volcanic arc where thin green tuffs called "lutita verde" are exploited by local communities. There is an indication that these tuffs have been reworked after the initial eruptive and depositional volcanic cycle. These tuffs mostly belong to the heulandite-clinoptilolite solid solution series with variable zeolite composition (Machiels et al. 2008). The Lower Cayo formation consists primarily of volcanic breccia, tuffs, and some basaltic lavas, while the Upper Cayo formation is "dominated by more sedimentary lithologies" (Masucci and Macfarlane 1997:770).

Accounting for the distance between these formations and our study area, the presence of the seasonally flowing rivers stemming from the mountains results in the fluvial transport of some of the geologic material found in these mountain formations (Masucci and Macfarlane 1997:773). In particular, variability between the movements of north-flowing and south-flowing ocean currents periodically results in a catastrophic rainy season, known as El Niño. This phenomenon can contribute to heavy erosion and movement of materials through river currents to the study area (Masucci and Macfarlane 1997:774; Reitz and Masucci 2004:41). The mineralogical makeup of the study area provides a baseline of locally and easily obtainable materials which may have been used to produce beads, and therefore can provide insight into the production and trade patterns of the Guangala and Manteño cultures.

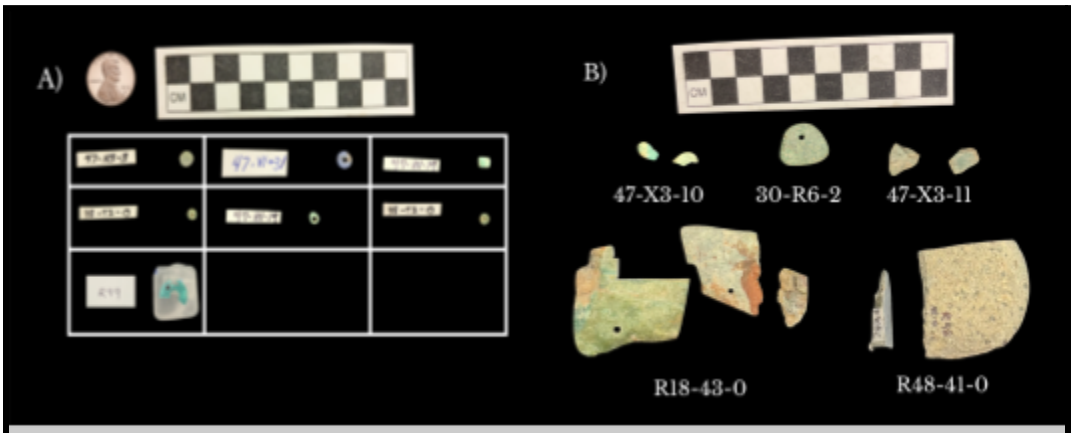

Figure 4: Images of all of our artifacts taken on a smartphone (A) Beads and beads in progress (B) Other non bead artifacts such as an axe and a pendant at varying stages of completion

Artifacts

Greenstone artifacts used for this study were found at a large Guangala site in El Azucar Valley, Ecuador, which is one of the largest concentrations of Guangala settlements (Masucci 1992). Selected beads were excavated from Site 47, a small Guangala farmstead and workshop,

or from adjacent Guangala settlements with evidence of bead manufacture. The beads in **Figure 4A** were selected for their green color, as well as a single blue bead. Other beads or greenstone fragments in stages of production were selected and included since our study aimed at investigating the use of greenstone in bead production. Shown in **Figure 4B**, a greenstone pendant and axe head were also selected due to the ability to create thin sections for petrographic analysis.

METHODOLOGY

Fourier Transform Infrared Spectroscopy with Attenuated Total Reflectance (FT-IR-ATR) coupled with optical petrography was used to identify the composition of the rock samples and selected artifacts. FT-IR-ATR generated a spectrum unique to each sample, which aided in determining their chemical compositions. Petrographic microscopy was used to identify minerals of the selected samples.

Fourier Transform Infrared Spectroscopy with Attenuated Total Reflectance (FT-IR-ATR)

A Thermo-Scientific Nicolet iS10 FT-IR attached with a Smart iTR™ Attenuated Total Reflectance Sampling accessory was used for the FT-IR analysis; a wavenumber range of 600 to 4000 cm^{-1} was used for spectral analysis. The ATR attachment directs an infrared laser that propagates through a crystal to the sample. The infrared light vibrates the chemical bonds in the sample, causing them to vibrate, allowing for analysis via a wavenumber spectrum. FT-IR-ATR is a non-destructive technique for the identification of solid samples, and it is a valuable technique in archaeology because of the minimal sample pre-processing involved. However, several sections of the river rock samples were determined to be common and cut with a gem saw for FT-IR-ATR analysis. Powder samples of select artifacts and rock samples were then prepared with a clean mortar and pestle. Although a destructive technique, pulverization of the samples was done to provide a more homogenous sample for FT-IR-ATR analysis. Each solid sample was analyzed with an FT-IR-ATR instrument three times in different locations along the surface. Each powdered sample was tested once. Out of each set of spectra collected from each sample, the spectra with the least apparent noise were used to determine the chemical composition of the rock.

Petrography

A petrographic microscope was used to analyze the mineral components of the local raw material samples and artifact thin sections. A Leica DM2500 P microscope showed each sample under both plane-polarized and cross-polarized light. Plane-polarized light that enters birefringent crystals attains a phase difference between s and p polarized light (University of Cambridge n.d.). When viewed under the cross-polarized setting, a second polarizer that is perpendicular to the first polarizer is used. This allows the different waves to be recombined and shows certain optical properties of the mineral crystals, such as birefringence. Each thin section sample was prepared at a standard 30 μm and analyzed at 40x, 100x, and 200x magnifications.

Hydrochloric Acid Test

A hydrochloric acid (HCl) test was also used to determine whether carbonates were present in certain samples. Calcite, or calcium carbonate ($CaCO_3$), if present, reacts with HCl

according to Reaction 1, shown in Figure 5. Also, malachite and dolomite are carbonate-based rocks that react similarly to calcite, shown in Reactions 2 and 3, respectively. One product of the reaction is gaseous carbon dioxide (CO_2). If carbonate is present, effervescence of CO_2 will be observed on the contact surface. If no carbonate is present, no reaction will occur with the hydrochloric acid. Due to unique bond strengths and chemical properties, each rock requires a different molar concentration of HCl to react. Therefore, by comparing the molar concentration that elicited a reaction on the samples, information can be gained regarding the composition of rocks.

Reaction 1

$$CaCO_3(s) + 2\,HCl(aq) \longrightarrow CaCl_2(aq) + H_2O(l) + CO_2(g)$$

Reaction 2

$$Cu_2CO_3(OH)_2(s) + 4\,HCl(aq) \longrightarrow 2\,CuCl_2(aq) + 4\,H_2O(l) + 2\,CO_2(g)$$

Reaction 3

$$CaMg(CO_3)_2(s) + 4\,HCl(aq) \longrightarrow CaCl_2(aq) + MgCl_2(aq) + 2\,H_2O(l) + 2\,CO_2(g)$$

Figure 5: The reactions that were used to determine mineral identity with the acid test.

ANALYSES

FT-IR-ATR

Both solid samples and powder samples were analyzed. Solid samples were tested multiple times if a reading was unclear, and provided an analysis of a small region of the artifact. Powder samples were first cut with a gem saw and then ground with a mortar and pestle. After testing the powdered samples with FT-IR-ATR, the instrument was cleaned with acetone and a cotton pad.

Correlational Analysis

For effective visualization and interpretation of the FT-IR data, a custom Python-based graphical user interface (GUI) was developed using Anaconda Jupyter and Visual Studio Code. In addition to reference spectra sourced from the RRUFF Project and the National Institute of Standards and Technology (NIST) Chemistry WebBook, the tool was designed to directly process and store proprietary Thermo-Scientific spectra files into readable comma-separated values. This optimized workflow ensured a consistent and reproducible method of spectral comparison through data analysis and figure generation.

Preliminary visual inspection focused on absorbance peak positions and shapes to identify mineral signatures. Quantitative comparisons were conducted using two statistical methods: Pearson's correlation coefficient (r) and Spearman's rank correlation coefficient (ρ).

1. Pearson correlation coefficient (r)

$$r = \frac{\Sigma(x_i - \bar{x})(y_i - \bar{y})}{\sqrt{\Sigma(x_i - \bar{x})^2 (y_i - \bar{y})^2}} \quad (1)$$

r = Pearson correlation coefficient
x_i, y_i = individual values
$\bar{x}$, $\bar{y}$ = mean values

2. Spearman correlation coefficient (ρ)

$$\rho = 1 - \frac{6\Sigma d_i^2}{n(n^2 - 1)} \quad (2)$$

ρ = Spearman rank correlation coefficient
d_i = difference between the two ranks of each observation
n = number of observations

Pearson's r captured overall similarity in spectral trends, emphasizing dominant features, while Spearman's ρ evaluated the alignment of local absorbance peaks regardless of intensity. Used together, these methods provide a robust, complementary assessment of spectral compatibility (Henschel et al. 2019). Each sample was run against 13 different minerals identified through qualitative analysis of FT-IR spectra: actinolite, albite, calcite, dolomite, jadeite, malachite, microcline, muscovite, orthoclase, phlogopite, quartz, sanidine, and turquoise. The resulting r and the ρ values were then ranked to generate a ranked-order compatibility table (**Table IA-ID**), returning the most likely mineral matches for each sample.

Petrography

A petrographic microscope, equipped with both plane-polarized light and cross-polarized light settings, allowed for qualitative observations of selected samples in thin sections. Thin sections were prepared by encasing our samples in resin and subsequently cutting thin sections of 30μm thickness. Specific qualities examined include birefringence through the Michel-Lévy interference chart, extinction angles, and the grains of thin sections. Photos of each sample were taken using an iPhone camera. Observations made through the petrographic microscope were compared to petrographic microscope photos of known rock samples, as well as to each other. Our identification of the samples relied on Longman Scientific & Technical atlases of metamorphic, igneous, and rock-forming minerals (Yardley et al. 1990; MacKenzie et al. 1982; Mackenzie et al. 1980).

Hydrochloric Acid Test

The hydrochloric acid test served as a final test for samples that were similar to the spectra or petrographic imaging for carbonates. Each sample suspected to contain a carbonate-based rock was tested with 0.1 M, 1.0 M, and 3.0 M hydrochloric acid, which would react from calcite, dolomite, and malachite, respectively. As a separate control, the carbonate-free granite was used as it would have no reaction. There was no evidence of released gas from the granite.

ArcGIS Pro Software

The ArcGIS Pro software was used to analyze geographic and geologic features within and around our sampling locations. Maps of Ecuador's waterways and geology, as well as maps of the sample locations, were overlayed on a basemap using a PWGS 1984 Web Mercator projection. Data from archaeological surveys of Manteño and Guangala settlements was also collected and visualized to understand their cultures as well as the overall importance of the region (Stothert, Masucci, and Carter 2008). In addition, a map of Ecuador was referenced within the software to provide an accurate way to identify nearby geological features.

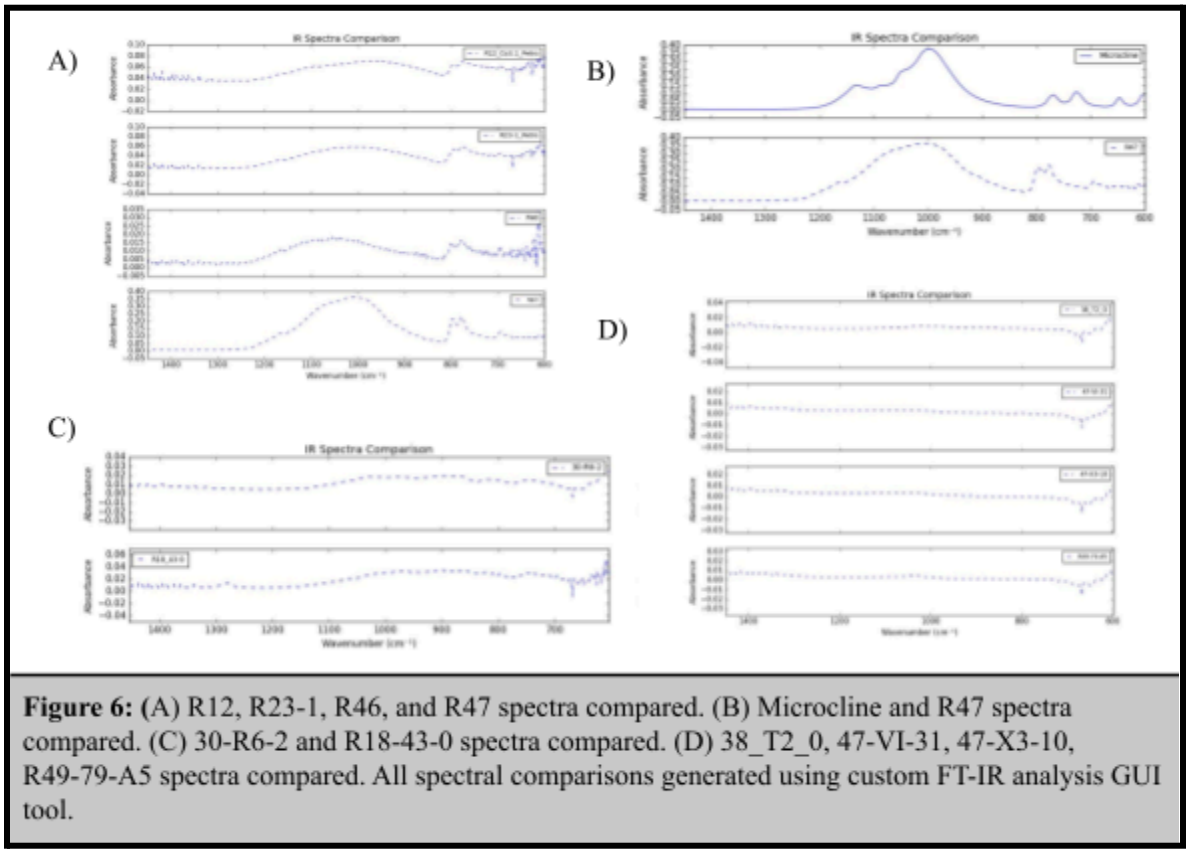

Figure 6: (A) R12, R23-1, R46, and R47 spectra compared. (B) Microcline and R47 spectra compared. (C) 30-R6-2 and R18-43-0 spectra compared. (D) 38_T2_0, 47-VI-31, 47-X3-10, R49-79-A5 spectra compared. All spectral comparisons generated using custom FT-IR analysis GUI tool.

RESULTS

Analysis of FT-IR-ATR spectra and petrographic images identified several samples related in composition. Rocks related to the Cayo formation likely have the same composition (Figure 6A). The spectra for these samples all had similar peaks around 1009, 796, 778, 695, and 1163. The spectra for these samples were very similar to the FT-IR-ATR spectrum of microcline, suggesting microcline as a possible mineral present in the samples. The spectrum of the Cayo formation rock was similar to the spectrum of microcline (Figure 6B). Petrographic analysis of Cayo formation rock was similar to petrographic imaging of microcline, but also suggested the samples could be composed of a mixture of silicates (feldspar, micas) or carbonates (quartz, calcite). Spectra for the two greenstone pendants are related as well (Figure 6C). Both have similar peaks at 740, 821, 896, and 969, again proposing similar compositions. The overlaid spectroscopies of the blue and green beads showed that the beads that vary in color are most

likely made of the same mineral composition (Figure 6D). Even though the colors are different between the beads, it is not a determining factor for its composition. Before physically relating the peaks using the spectra, we made previous qualitative inferences by visibly identifying the minerals determining general classes and potential minerals.

Table IA. Artifacts ranked by probability of tested minerals based on Pearson correlation

Provenience	First Most Probable Mineral (r ≈ .xx)	Second Most Probable Mineral (r ≈ .xx)	Third Most Probable Mineral (r ≈ .xx)
R18_43-0_IR_S_G3 #3	Paragonite (r ≈ .87)	Muscovite (r ≈ .83)	Phlogopite (r ≈ .81)
R48_41-0_IR_S_G2 #1	Muscovite* (r ≈ .82)	Phlogopite (r ≈ .80)	Paragonite (r ≈ .79)
R49-79-A5_IR_S_G1_#2	Quartz (r ≈ .60)	Turquoise (r ≈ .59)	Sanidine (r ≈ .46)
47-X3-10_IR_S_G1_#1	Quartz (r ≈ .42)	Calcite (r ≈ .41)	Turquoise (r ≈ .37)
47-H1-19_IR_S_G1_#1	Malachite* (r ≈ .74)	Muscovite (r ≈ .72)	Jadeite (r ≈ .56)
47-H3-3_IR_S_G1_#1	Orthoclase (r ≈ .94)	Sanidine (r ≈ .93)	Microcline (r ≈ .92)
38-T2-0_IR_S_G1_#1	Quartz (r ≈ .56)	Turquoise (r ≈ .53)	Sanidine (r ≈ .42)
30-R6-2_IR_S_G1_#1	Paragonite (r ≈ .91)	Muscovite (r ≈ .86)	Jadeite (r ≈ .84)
47-VI-31_IR_S_G1_#4	Calcite (r ≈ .52)	Dolomite (r ≈ .47)	Sanidine (r ≈ .19)

Table IB. Artifacts ranked by probability of tested minerals based on Spearman correlation

Provenience	First Most Probable Mineral (ρ ≈ .xx)	Second Most Probable Mineral (ρ ≈ .xx)	Third Most Probable Mineral (ρ ≈ .xx)
R18_43-0_IR_S_G3 #3	Muscovite (ρ ≈ .91)	Phlogopite (ρ ≈ .81)	Jadeite (ρ ≈ .79)
R48_41-0_IR_S_G2 #1	Muscovite* (ρ ≈ .84)	Phlogopite (ρ ≈ .82)	Jadeite (ρ ≈ .79)
R49-79-A5_IR_S_G1_#2	Calcite (ρ ≈ .47)	Malachite (ρ ≈ .45)	Turquoise (ρ ≈ .43)
47-X3-10_IR_S_G1_#1	Calcite (ρ ≈ .62)	Turquoise (ρ ≈ .57)	Jadeite (ρ ≈ .27)
47-H1-19_IR_S_G1_#1	Malachite* (ρ ≈ .86)	Turquoise (ρ ≈ .73)	Muscovite (ρ ≈ .65)
47-H3-3_IR_S_G1_#1	Muscovite (ρ ≈ .93)	Albite (ρ ≈ .91)	Jadeite (ρ ≈ .90)
38-T2-0_IR_S_G1_#1	Calcite (ρ ≈ .51)	Malachite (ρ ≈ .45)	Turquoise (ρ ≈ .44)
30-R6-2_IR_S_G1_#1	Jadeite (r ≈ .93)	Muscovite (r ≈ .882)	Phlogopite (ρ ≈ .881)
47-VI-31_IR_S_G1_#4	Turquoise (ρ ≈ .64)	Calcite (ρ ≈ .63)	Malachite (ρ ≈ .01)

Table IC. Rocks ranked by probability of tested minerals based on Pearson correlation

Provenience	First Most Probable Mineral (r ≈ .xx)	Second Most Probable Mineral (r ≈ .xx)	Third Most Probable Mineral (r ≈ .xx)
R09_Petro_Z13.1_IR_P_G3#1	Lizardite (r ≈ .75)	Paragonite (r ≈ .66)	Actinolite (r ≈ .64)
R12_Co3.1_Petro_IR_S_G3_#1	Muscovite* (r ≈ .85)	Paragonite (r ≈ .784)	Phlogopite (r ≈ .779)
R47_IR_P_G1 #1	Orthoclase* (r ≈ .93)	Sanidine (r ≈ .914)	Microcline (r ≈ .911)
R46_IR_P_G1 #1	Quartz* (r ≈ .91)	Turquoise (r ≈ .88)	Orthoclase (r ≈ .77)
R23-1_Petro_IR_S_G3 #1	Muscovite (r ≈ .82)	Orthoclase (r ≈ .78)	Microcline (r ≈ .76)
R23-2_Petro_IR_S_G2 #1_Co.11.2	Orthoclase* (r ≈ .92)	Muscovite (r ≈ .911)	Sanidine (r ≈ .906)
510-0_IR_S_G2#3	Paragonite (r ≈ .97)	Actinolite (r ≈ .91)	Jadeite (r ≈ .90)

Table ID. Rocks ranked by probability of tested minerals based on Spearman correlation

Provenience	First Most Probable Mineral (ρ ≈ .xx)	Second Most Probable Mineral (ρ ≈ .xx)	Third Most Probable Mineral (ρ ≈ .xx)
R09_Petro_Z13.1_IR_P_G3#1	Actinolite (ρ ≈ .49)	Paragonite (ρ ≈ .46)	Lizardite (ρ ≈ .45)
R12_Co3.1_Petro_IR_S_G3_#1	Muscovite* (ρ ≈ .90)	Actinolite (ρ ≈ .86)	Phlogopite (ρ ≈ .85)
R47_IR_P_G1 #1	Orthoclase* (ρ ≈ .940)	Sanidine (ρ ≈ .937)	Microcline (ρ ≈ .93)
R46_IR_P_G1 #1	Quartz* (ρ ≈ .96)	Sanidine (ρ ≈ .877)	Microcline (ρ ≈ .876)
R23-1_Petro_IR_S_G3 #1	Orthoclase (ρ ≈ .88)	Sanidine (ρ ≈ .87)	Microcline (ρ ≈ .86)
R23-2_Petro_IR_S_G2 #1_Co.11.2	Orthoclase* (ρ ≈ .911)	Actinolite (ρ ≈ .909)	Lizardite (ρ ≈ .897)
510-0_IR_S_G2#3	Lizardite (ρ ≈ .954)	Paragonite (ρ ≈ .948)	Actinolite (ρ ≈ .93)

After finding peaks and potential minerals, correlation analysis was used to draw quantitative conclusions where separate methods helped cross-validate the results. Ranked order Pearson and Spearman correlation exhibited the highest correlated minerals and samples (**Table IA, IB, IC, ID**). Orthoclase, muscovite and quartz were the most frequent highest correlated minerals for artifacts. Rocks were more diversified in their correlated minerals with calcite and quartz with highest frequency as the highest ranked correlation, whose dissimilarity is attributed to the differences in each correlation method. Artifacts and rocks had multiple overlap in highly correlated minerals including muscovites, calcites, paragonites, quartz, calcites, and orthoclases (**Table IA, IB, IC, ID**).

Table II.

Acid Test Results						
Yes: Effervescence No: No reaction		Artifact				
		R47-H1-19	R49-79-A5	38-T2-0	R18-43-0	30-R6-2
Molarities	0.1M	Yes	Yes	No	No	Yes
	1.0M	Yes	Yes	No	No	Yes
	3.0M	Yes	Yes	Yes	No	Yes

The acid test helped determine the presence of carbonates such as calcite, dolomite, and malachite in any suspected rocks. The petrographic microscope displayed high interference colors in the cross-polarized light, but not in plane-polarized light for both pendants. We tested both of the greenstone pendants, 30-R6-2 and R18-43-0; and 3 beads, 38-T2-0, 47-H1–19, and R49-79-A5. After performing the acid test, three artifacts - two beads and one pendant - effervesced in HCl suggesting the presence of calcite (**Table II**).

Table IIIA. Artifact samples description and potential identities.

Provenience	Artifact Color	Artifact Type	FT-IR (powder or solid)	Notable Peak Locations (cm-1)	Potential Minerals
R18_43-0_IR_S_G3 #3	Green	Pendant	Solid	1278, 968, 897, 867, 816, 750	Micas (Paragonite)
R48_41-0_IR_S_G2 #1	Grey/Beige	Axe	Solid	1107, 1000, 884	Micas (Muscovite, Phlogophite/Biotite, Paragonite)
R49-79-A5_IR_S_G1_#2	Green	Bead	Solid	1319, 1245, 1175, 1109, 1036, 824	Quartz, Calcite
47-X3-10_IR_S_G1_#1	Green	Stone Fragment	Solid	675, 660, 640 635, 625, 615, 610,	Carbonate (Calcite), Silicate (Quartz)
47-H1-19_IR_S_G1_#1	Green	Bead	Solid	1097, 1028, 1017, 875, 816, 773, 748, 713	Carbonate (Calcite, Malachite)
47-H3-3_IR_S_G1_#1	Green	In-Process Bead	Solid	1102, 1033, 986, 897, 833, 779, 691	Orthoclase feldspar (Sanidine, Microcline)
38-T2-0_IR_S_G1_#1	Green	Bead	Solid	1315, 1035	Carbonate, Quartz, Turquoise
30-R6-2_IR_S_G1_#1	Green	Pendant	Solid	1065, 1028, 1017, 968, 876, 892, 818, 743, 716	Micas (Paragonite, Muscovite), Jadeite, Carbonates
47-VI-31_IR_S_G1_#4	Blue	Bead	Solid	1035, 920, 730, 715	Carbonate (Calcite, Dolomite)

Table IIIB. Rock samples description and potential identities.

Provenience	Rock Color	Sampling Location	FT-IR (powder or solid)	Notable Peak Locations (cm-1)	Potential Minerals
R09_Petro_Z13.1_IR_P_G3#1	Gray	Baja Alburrada de Calicanto	Powder	1100, 943, 750	Lizardite, Micas (Paragonite, Actinolite/Nephrite)
R12_Co3.1_Petro_IR_S_G3_#1	Gray/Brown	Aguadita	Solid	1160, 1091, 963, 792, 777, 692	Silicate, Micas (Biotite/Plogophite/Muscovite), Actinolite
R47_IR_P_G1 #1	Green	Rock in Salango Clay sample	Powder	1163, 1008, 796, 777, 694	Orthoclase Feldspar (Sanidine, Microcline)
R46_IR_P_G1 #1	Brown-Orange/Gray	Los Cebitos - loose rock	Powder	1082, 1048, 801, 778, 757, 695, 638, 617	Quartz
R23-1_Petro_IR_S_G3 #1	Green	Rio de las Cañas	Solid	1165, 1008, 796, 779, 694	Orthoclase feldspar, Silicates (Muscovite, Microcline)
R23-2_Petro_IR_S_G2 #1_Co.11.2	Gray/Beige	Rio de las Cañas	Solid	994, 875	Silicates (Orthoclase, Muscovite)
510-0_IR_S_G2#3	Gray/Green	Greenstone fragments	Solid	1201, 1037, 940, 780, 672, 652	Mica (Paragonite), Lizardite, Actinolite

Through multimodal parallel analysis utilizing correlation analyses (Pearson and Spearman), petrographic thin sections, and FT-IR qualitative peak analysis, we were able to distinguish the most probable minerals and identity of the rock and artifact samples. In all samples, we determined the composition to consist of silicate or carbonate minerals. Of the silicates, 9 samples of 4 artifacts and 5 local rocks (**Table IIIA and IIIB**) contain minerals of the

mica family. Furthermore, analysis of the R09 petrographic thin section suggests a basaltic and siltstone composition for R12.

An additional overlap in sample composition lied within orthoclase feldspars which was both present in an in-process bead artifact (47-H3-3) and two local rock samples (**Table IIIA and IIIB**). A majority of samples consist of the silica (O-Si-O) bond peak between 900-1100 wavenumbers (cm^{-1}). On the contrary, carbonate materials were found in a few beads with few in the form of calcite or carbon bonds in the FT-IR-ATR peaks 800-1400. For sample 47-H1-19, the FT-IR-ATR correlation analysis had a strong association with malachite; however, the sample's identity as calcite was supported by the effervescing in HCl (**Table IIIA**). Furthermore, there were few varied correlations between alternate minerals such as the lizardite (serpentinite), actinolite (nephrite), jadeite, turquoise, and dolomite.

DISCUSSION

Geologic Background

We determined that although most of the artifacts had varied compositions, many overlapped with local stones, specifically with micas, orthoclase feldspars, quartz, and carbonates (**Tables IA-D, Tables IIIA&B**). These minerals are commonly found in Ecuadorian geologic formations: the Santa Elena Olistostromic Complex in Ecuador borders archaeological villages near El Azucar which contain quartz, muscovite, and basalt; the Tosuagua formation with two members near sites with the Zapotal member containing quartz, plagioclase, and biotite; and the Dos Bocas consisting of plagioclase, muscovites, and siltstones (**Figure 7**). The presence of quartz and carbonates is compatible with the Guangala and Manteño coastal landscape surrounded by the Piñon and Cayo formation, which contain marine and sedimentary-based carbonate rocks. Actinolite (and in fewer quantities, nephrite) can be found in the Camilo Ponce Enríquez Canton from the Azuay Province in Ecuador, although in limited quantities as inclusions in rocks. Serpentinite and lizardite is often found in ultramafic formations throughout the Andes, while turquoise and jadeite are not known to be found in Ecuador in substantial quantities. Our results in the geologic context suggest that the greenstone beads could have been predominantly composed of local green-colored stone.

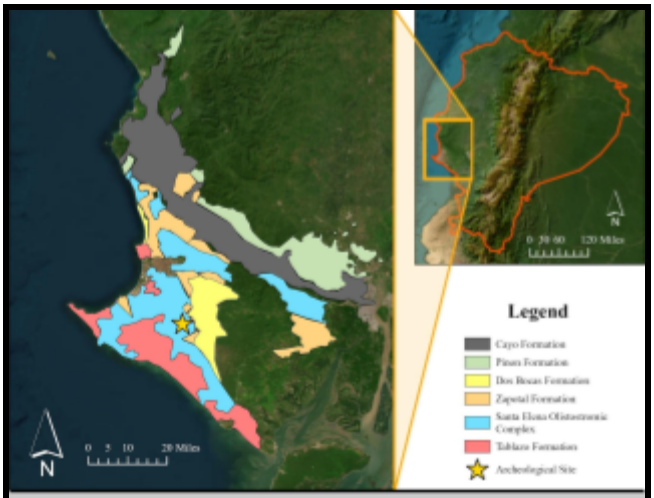

Figure 7: Six local geologic formations to our archeological site in southwestern Ecuador.

Guangala and Manteño Society

This study offers insight on the culture and practices of the Guangala and Manteño. If the beads were composed of different materials, as suggested by the results, it would indicate that the materials were chosen due to similar visual properties rather than for the material itself. This provides insight into the value system of pre-Columbian cultures. In particular, it infers that value was not necessarily restricted to modern valued minerals, such as jadeite and gold. Instead, it suggests that the cultural significance of the color alone could elevate the value of these materials and artifacts. Accepting that the artifacts are composed of local materials, it is likely that the raw materials were collected rather than imported through trade. This also supports the understanding that the beads were produced locally. It aligns with the theory that the beads were used as an economic export, as production using local materials would allow for further margins of profit (Masucci 1995).

Due to correlations with non-local materials such as jadeite and turquoise, one must take into account the possibility of the importation of the raw materials used for production. Accepting that the beads were produced in Ecuador, as the evidence suggests, raises questions about the theory that they were produced primarily for an export purpose. In particular, it raises questions about the motive behind the importations. What was keeping other Pre-Columbian cultures from producing the beads themselves? Did Guangala and Manteño have more advanced technology and production methods than surrounding cultures, which attracted other peoples to their work quality? These questions can be explored through future studies and would expand archaeologists' understanding of the unique role of Guangala society within the wider pre-Columbian network. It is also possible that the production was not as centralized in coastal Ecuador as currently thought, and further investigation may provide more insight.

Methodology

In our study we utilized a novel multimodal approach which compared petrographical images in cross- and plane-polarized light, FT-IR-ATR spectra of powders and solids, HCl acid tests, and correlation analysis of relevant minerals. This allowed for a multifaceted analysis to determine the identity of our samples. There is also novelty in the utilization of Pearson and Spearman analysis on FT-IR-ATR spectroscopy in an archaeological context; these analyses showed similarities with qualitative observations, which helped confirm results. This method allowed for a more comprehensive cross-validation of each qualitative and quantitative strategy.

In addition to having implications on the current understanding of Guangala and Manteño societies, this study contributes to the future of non-destructive research in archaeology. This study has shown that non-destructive analysis of samples is possible. FT-IR-ATR spectroscopy was effective with non-destroyed solid samples, although it sometimes required multiple readings to show a definitive spectra. These spectra had clear peaks and could easily be compared to the spectra of other minerals, which helped samples be identified. While FT-IR-ATR spectroscopy was useful, the acid test and petrography were necessary to provide a different perspective and validate results. In future studies, researchers should utilize FT-IR-ATR spectroscopy as well as other non-destructive methods of analysis; however, destructive methods may still be needed for definite conclusions. To lessen the impact of destructive methods, researchers should strive to preserve samples with historic and cultural significance and to destroy samples with less significance or those that are more common.

Limitations

In the duration of our study, there were variables and aspects that impacted the confidence and range of our research. Archaeological samples constantly undergo weathering and compositional changes due to their age and burial conditions, including the formation of a calcium carbonate outerlayer, impacting results of correlation, FT-IR, and acid test analysis (Merill 1896:717; Sáenz-Martínez 2019). Variation across each analytical method can be attributed to variations in each trial and subjectivity in qualitative analysis of petrography and FT-IR spectra. The correlation analysis was limited in its manualization and compatibility. The quantities of our samples and data were limited by time access and variation due to sampling chance must be taken into consideration, along with our lack of ability to produce thin sections of the greenstone beads for petrographic analysis comparison.

CONCLUSION

Around the globe, greenstone beads have been found in burial and ritual contexts, suggesting their cultural significance as symbols of wealth and status. Our study analyzed the composition of greenstone beads from production sites in Guangala and Manteño settlements in the southwestern coastal region of Ecuador. Understanding the origin and composition of these beads is essential to understanding the history of pre-Columbian societal structure and cross-cultural trade.

Our study yielded a variety of mineral compositions in both the local greenstone raw materials and the artifacts that were mostly present in the geologic formations in the area of study. The differing mineral compositions suggest that the Guangala and Manteño people did not

focus on the material of their greenstone beads; instead, they focused on the green appearance. Consequently, our study provides a unique insight into the cultures and economic strategies of these groups. While the study yielded significant results, it would be beneficial to further pursue the study of greenstone beads. These beads have immense cultural significance, and given more time to broaden the scope of our research, greater findings could be made. This study had a limited timeframe, and future research could utilize more non-destructive methods of analysis as well as more in-depth comparisons between minerals and artifacts from surrounding areas. This could further uncover if the thousands of greenstone beads in burials at other sites were produced by Ecuadorian workshops. Further, it is now clear that archaeologists must exercise caution in identifying greenstone materials without actual mineralogical or chemical analyses. These tiny greenstone beads are an exciting window into the history of Guangala and Manteño cultures, and the larger geographical context of ancient Latin America.

In the scope of archaeological research, our study provides a novel methodology in the analysis of artifacts. Both non-destructive and destructive techniques of analysis, including FT-IR-ATR analysis, petrographic analysis, and acid reaction tests, were utilized. The novel application of Pearson and Spearman's correlation analysis for FT-IR spectra on artifact and rock samples revealed a potential for its effective utilization in archaeology. Extending beyond FT-IR, other chemical instruments, including Raman spectroscopy, X-ray fluorescence, and X-ray diffraction, could be utilized to increase understanding of historical objects. By cross-analyzing qualitative petrographic images, acid testing, and FT-IR spectra with quantitative computational analysis, our study highlights the value of similar multimodal approaches in an archaeological lens.

Acknowledgements

We would like to acknowledge Novartis Pharmaceuticals Corp., Bristol Myers Squibb, the Overdeck Family Foundation, the State of New Jersey: Office of the Secretary of Higher Education, and all other alumni and supporters of GSNJS. We are also grateful to Dr. Adam Cassano and Dr. Steve Dunaway for their leadership and support. Finally, we would like to thank our advisor Dr. Maria Masucci for her guidance and expertise, and our mentors Ece Onatca and Katelyn Rohlf for their assistance on the project.

Bibliography

"Actinolite from Azuay Province, Ecuador." Mindat.org. Accessed July 23, 2025. https://www.mindat.org/locentries.php?p=131952&m=18.

Aguilar-Melo, Valentina, Alejandro Mitrani, Edgar Casanova-Gonzalez, et al. "Molecular and X-ray Spectroscopies for Noninvasive Characterization of Mayan Green Stones from Bonampak, Chiapas." *Applied Spectroscopy* 73, no. 9 (2019): 1074-86. Accessed July 12, 2025. https://doi.org/10.1177/0003702819848478.

Aizprua, Carlos, C. Witt, M. Brönner, S. E. Johansen, D. Barba, and M. J. Hernandez. "Forearc Crustal Structure of Ecuador Revealed by Gravity and Aeromagnetic Anomalies and Their Geodynamic Implications." *Lithosphere* 2020, no. 1 (2020). Accessed July 12, 2025. https://doi.org/10.2113/2020/2810692.

Boomert, Arie. "Gifts of the Amazons: 'green stone' pendants and beads as items of ceremonial exchange in Amazonia and the Carib bean." *Antropologica* 67 (1987): 33-54. Accessed July 12, 2025. https://biblat.unam.mx/hevila/AntropologicaCaracas/1987/no67/2.pdf.

Cabera, Jonathan Santana, Erik López Reyes, Domingo C. Salazar García, Lourdes Colcha Guamán, and Juan Abella Pérez. "New Bioarchaeological Evidence for Guangala and Manteño-Huancavilca Cultures in Santa Elena Peninsula (Southern Ecuadorian Coast)." In *The 80th Annual Meeting of the Society for American Archaeology*. 2015. Accessed July 12, 2025. https://core.tdar.org/document/398131/new-bioarchaeological-evidence-for-guangala-and-manteno-huancavilca-cultures-in-santa-elena-peninsula-southern-ecuadorian-coast.

Carter, Benjamin, and Matthew Helmer. "Elite Dress and Regional Identity: Chimú-Inka Perforated Ornaments from Samanco, Nepeña Valley, Coastal Peru." *Beads: Journal of the Society of Bead Researchers* 27 (2015): 46-74. Accessed July 12, 2025. https://surface.syr.edu/beads/vol27/iss1/1.

Chiaradia, Massimo, Lluís Fontbote, Agustín Paladines, and Bernardo Beate. "Ore Deposits, Magmas and Tectonism in Ecuador." *Congreso Latinoamericano de Geología, Memorias* 12 (2005): 5. Accessed July 16, 2025. https://app.ingemmet.gob.pe/biblioteca/pdf/CLG12-10.pdf.

Currie, Elizabeth J. "Archaeology, Ethnohistory and Exchange along the Coast of Ecuador." *Antiquity* 69, no. 264 (1995): 511-26. Accessed July 23, 2025. https://doi.org/10.1017/s0003598x00081904.

Delgado Robles, Alma A., Jose Luis Ruvalcaba Sil, Pieterjan Claes, et al. "Non-destructive in Situ Spectroscopic Analysis of Greenstone Objects from Royal Burial Offerings of the Mayan Site of Palenque, Mexico." *Heritage Science* 3, no. 1 (2015). Accessed July 23, 2025. https://doi.org/10.1186/s40494-015-0048-z.

Donoso-Tapia, Damián, Kennet E. Flores, Celine Martin, Esteban Gazel, and Jeffrey Marsh. "Exhumed Serpentinites and Their Tectonic Significance in Non-Collisional Orogens." *Geochemistry, Geophysics, Geosystems* 25, no. 2 (2024). Accessed July 23, 2025. https://doi.org/10.1029/2023gc011072.

Glavcheva, Z. I., D. Y. Yancheva, Y. K. Kancheva, E. Velcheva, and B. A. Stamboliyska. "Development of FTIR Spectra Database of Reference Art and Archaeological Materials." *Bulgarian Chemical Communications* 46, nos. Special Issue A (2014): 164-69. Accessed July 23, 2025. https://www.researchgate.net/profile/Denitsa-Yancheva/publication/291696406_Develop

ment_of_FTIR_spectra_database_of_reference_art_and_archaeological_materials/links/56e3d47908ae98445c1e4744/Development-of-FTIR-spectra-database-of-reference-art-and-archaeological-materials.pdf.
Gwinnett, A. John, and Leonard Gorelick. "A Brief History of Drills and Drilling." *BEADS: Journal of the Society of Bead Researchers* 10 (1998): 49-56. Accessed July 23, 2025. https://surface.syr.edu/beads/vol10/iss1/8/.
Henschel, Henning, Alfred T. Andersson, Willem Jespers, Mohammad Mehdi Ghahremanpour, and David van der Spoel. "Theoretical Infrared Spectra: Quantitative Similarity Measures and Force Fields." *Journal of Chemical Theory and Computation* 16, no. 5 (2020): 3307-15. Accessed July 23, 2025. https://doi.org/10.1021/acs.jctc.0c00126.
Juengst, Sara L., Sarah M. Rowe, Guy S. Duke, Mara Stumpf, Mozelle Bowers, and Y. Zindy Cruz. "An Enigmatic Manteño Burial from Buen Suceso, Ecuador, AD 771?953." *Latin American Antiquity*, January 23, 2025, 1-9. Accessed July 23, 2025. https://doi.org/10.1017/laq.2024.20.
Knight, Willow, Faith Gantz, Matthew Carl, et al. "Complementary Scientific Techniques for the Study of Mesoamerican Greenstone Objects." *Heritage Science* 12, no. 1 (2024). Accessed July 16, 2025. https://doi.org/10.1186/s40494-023-01128-7.
Kokaly, Raymond F., Roger N. Clark, Gregg A. Swayze, et al. "USGS Spectral Library Version 7." *Data Series*, 2017. Accessed July 12, 2025. https://doi.org/10.3133/ds1035.
Krynine, Paul D. "The Megascopic Study and Field Classification of Sedimentary Rocks." *The Journal of Geology* 56, no. 2 (1948): 130-65. http://www.jstor.org/stable/30070803.
MacKenzie, W. S., and C. Guilford. *Atlas of Rock-forming Minerals in Thin Section*. 5th ed. Longman, 1980. Accessed July 20, 2025. https://www.geokniga.org/bookfiles/geokniga-atlas-rock-forming-minerals-thin-section.pdf.
Manrique-Ortega, M. D., P. Claes, E. Casanova-González, J. L. Ruvalcaba-Sil, Ma A. García-Bucio, and L. Lowe. "Non-Invasive Analysis of Green Stone Pieces from Tomb 1 of Chiapa De Corzo, Chiapas." *MRS Proceedings* 1618 (2014): 17-29. Accessed July 12, 2025. https://doi.org/10.1557/opl.2014.452.
Masucci, Maria Ann. , 1992. "Ceramic Change in the Guangala Phase, Southwest Ecuador: A Typology and Chronology." Order No. 9225388, Southern Methodist University. http://ezproxy.drew.edu/login?url=https://www.proquest.com/dissertations-theses/ceramic-change-guangala-phase-southwest-ecuador/docview/304041933/se-2.
Masucci, Maria, and Allison Macfarlane. "An Application of Geological Survey and Ceramic Petrology to Provenance Studies of Guangala Phase Ceramics of Ancient Ecuador." *Geoarchaeology* 12, no. 7 (1997): 765-93. Accessed July 12, 2025. https://www.academia.edu/33511655/An_application_of_geological_survey_and_ceramic_petrology_to_provenance_studies_of_Guangala_phase_Ceramics_of_ancient_Ecuador.
Masucci, Maria A. "Early Regional Polities of Coastal Ecuador." *The Handbook of South American Archaeology*, 2008, 489-503. Accessed July 23, 2025. https://doi.org/10.1007/978-0-387-74907-5_25.
Masucci, Maria A. "Marine Shell Bead Production and the Role of Domestic Craft Activities in the Economy of the Guangala Phase, Southwest Ecuador." *Latin American Antiquity* 6, no. 1 (1995): 70-84. https://doi.org/10.2307/971601.
Merrill, George P. "The Principles of Rock Weathering." *The Journal of Geology* 4, no. 6 (1896): 704-24. http://www.jstor.org/stable/30054608.

National Institute of Standards and Technology. "Mica." NIST Chemistry WebBook. U.S. Department of Commerce. Last modified 2025. Accessed July 16, 2025. https://webbook.nist.gov/cgi/cbook.cgi?ID=B6004666&Mask=80.

Navarro, Alexandre Guida. "Greenstone Pendants (Muiraquitãs): Spheres of Political Interaction among the Caribbean, Lower Amazon and Maranhão, Brazil." *Global Journal of Archaeology & Anthropology* 13, no. 5 (2024). Accessed July 12, 2025. https://doi.org/10.19080/gjaa.2024.13.555873.

Odokuma-alonge, Ovie, and Susan Chioma D?ban?. "Geochemical and Petrographic Studies of Some Quartz Mica Schists in Igarra and Environs, Southwestern Nigeria." *International Journal of Earth Sciences Knowledge and Applications* 4, no. 3 (2022): 476-85. Accessed July 16, 2025. https://dergipark.org.tr/en/pub/ijeska/issue/74681/1227287.

"The Origins of Jade | Nephrite, Jadeite, and More!" Video, 7:52. YouTube. Posted by Gemstones, February 24, 2022. Accessed July 12, 2025. https://www.youtube.com/watch?v=LpQoaYZ0x8o.

Ozpinar, Yahya, Baris Semiz, and Paul A. Schroeder. "Zeolites in Mafic Pyroclastic Rocks from the Sandikli-Afyonkarahisar Region, Turkey." *Clays and Clay Minerals* 61, no. 3 (2013): 177-92. Accessed July 16, 2025. https://doi.org/10.1346/ccmn.2013.0610302.

Perkins, Dexter. "Epidote-Clinozoisite." Optical Mineralogy. Accessed July 16, 2025. https://sites.und.edu/dexter.perkins/opticalmin/epidote.htm.

Petit, Tristan, and Ljiljana Puskar. "FTIR Spectroscopy of Nanodiamonds: Methods and Interpretation." *Diamond and Related Materials* 89 (October 2018): 52-66. Accessed July 20, 2025. https://doi.org/10.1016/j.diamond.2018.08.005.

"Petrography and Mineralogy of Zeolite Deposits, Mareya Area Southwest Thamar, Yemen." *Current Science International* 7, no. 2 (2018): 204-12.

Piperno, Dolores R., and Karen E. Stothert. "Phytolith Evidence for Early Holocene Cucurbita Domestication in Southwest Ecuador." *Science* 299, no. 5609 (2003): 1054-57. Accessed July 23, 2025. https://doi.org/10.1126/science.1080365.

Queffelec, Alain, Pierrick Fouéré, Céline Paris, Christian Stouvenot, and Ludovic Bellot-Gurlet. "Local Production and Long-distance Procurement of Beads and Pendants with High Mineralogical Diversity in an Early Saladoid Settlement of Guadeloupe (French West Indies)." *Journal of Archaeological Science: Reports* 21 (October 2018): 275-88. Accessed July 23, 2025. https://doi.org/10.1016/j.jasrep.2018.07.011.

Raymond, J. Scott, Richard L. Burger, and Jeffrey Quilter. *Archaeology of Formative Ecuador : a Symposium at Dumbarton Oaks, 7 and 8 October 1995*. Dumbarton Oaks Research Library and Collection, 2003. Accessed July 12, 2025. https://ia803408.us.archive.org/32/items/raymond-burger-archaeology-of-formative-ecuador/Raymond_Burger_Archaeology%20of%20Formative%20Ecuador.pdf.

Reitz, Elizabeth J., and Maria A. Masucci. "Guangala Fishers and Farmers: A Case Study of Animal Use at El Azúcar, Southwestern Ecuador" [Pescadores y Agricultores Guangala: Un Estudio de Caso de Uso Animal en El Azúcar, Suroeste de Ecuador]. *Latin American Archaeology* 14 (2004). Accessed July 12, 2025. https://sites.pitt.edu/~ccapubs/pdfdownloads/PITTmem14-Reitz_Masucci_2004.pdf.

Sáenz-Martínez, Á, M. San Andrés, M. Alvarez de Buergo, I. Blasco, and R. Fort. "Removing Calcium Carbonate Deposits from Archaeological Ceramics. Traditional Methods under Review." *Mediterranean Archaeology and Archaeometry* 19, no. 3 (2019): 107-17. Accessed July 23, 2025. https://doi.org/10.5281/ZENODO.3583061.

Saikia, Bhaskar J., and Gopalakrishnarao Parthasarathy. "Fourier Transform Infrared Spectroscopic Characterization of Kaolinite from Assam and Meghalaya, Northeastern India." *Journal of Modern Physics* 01, no. 04 (2010): 206-10. Accessed July 16, 2025. https://doi.org/10.4236/jmp.2010.14031.

Schmidt, Susanne Theodora. "The Petrographic Microscope: A Polarized Light Microscope." *Springer Textbooks in Earth Sciences, Geography and Environment*, 2023, 37-48. Accessed July 20, 2025. https://doi.org/10.1007/978-3-031-19612-6_3.

Selvan, G. Adaikala, S. Rachel, and T. Gajendran. "Several Assorted Characterization Methods of Nanoparticles." *Nanomaterials*, 2021, 301-08. Accessed July 12, 2025. https://doi.org/10.1016/b978-0-12-822401-4.00040-4.

Shepard, A.O., 1956. Ceramics for the Archaeologist (Vol. 609, p. 1971). Washington, DC: Carnegie Institution of Washington. Accessed July 21, 2025. https://exhibits.library.sc.edu/sc-pottery/wp-content/uploads/sites/7/2014/09/Shepard-Ceramics-for-the-Archaeologist.pdf

Shimada, Izumi. *Who Were the Sicán? Their Development, Characteristics and Legacies*. 2009. Accessed July 12, 2025.

Staller, John E., and Elizabeth J. Currie. *Mortuary Practices and Ritual Associations: Shamanic Elements in Prehistoric Funerary Contexts in South America*. University of Michigan Press, 2001. Accessed July 23, 2025. https://doi.org/10.30861/9781841712680.

Stanienda-Pilecki, Katarzyna J. "The Importance of Fourier-Transform Infrared Spectroscopy in the Identification of Carbonate Phases Differentiated in Magnesium Content." *Spectroscopy* 34, no. 6 (2019): 32-42. Accessed July 20, 2025. https://www.spectroscopyonline.com/view/spec0619-pilecki.

"Strength of Correlation." Newcastle University. Accessed July 20, 2025. https://www.ncl.ac.uk/webtemplate/ask-assets/external/maths-resources/statistics/regression-and-correlation/strength-of-correlation.html.

Taylor, J. C. M. "Impregnation of Rocks for Sectioning." *Geological Magazine* 97, no. 3 (1960): 261. Accessed July 12, 2025. https://doi.org/10.1017/s0016756800061458.

Tsai, De-Hao, Melissa Davila-Morris, Frank W. DelRio, Suvajyoti Guha, Michael R. Zachariah, and Vincent A. Hackley. "Quantitative Determination of Competitive Molecular Adsorption on Gold Nanoparticles Using Attenuated Total Reflectance?Fourier Transform Infrared Spectroscopy." *Langmuir* 27, no. 15 (2011): 9302-13. Accessed July 20, 2025. https://doi.org/10.1021/la2005425.

Tschegg, Cornelius, A. Hugh N Rice, Bernhard Grasemann, et al. "Petrogenesis of a Large-Scale Miocene Zeolite Tuff in the Eastern Slovak Republic: The Ni?ný Hrabovec Open-Pit Clinoptilolite Mine." *Economic Geology* 114, no. 6 (2019): 1177-94. Accessed July 16, 2025. https://doi.org/10.5382/econgeo.4679.

University of Cambridge. "Single Crystals: Optical Properties." Dissemination of IT for the Promotion of Materials Science. Accessed July 20, 2025. https://www.doitpoms.ac.uk/tlplib/atomic-scale-structure/single3.php.

Vallejo, Cristian, Santiago Almagor, Christian Romero, et al. "Sedimentology, Provenance and Radiometric Dating of the Silante Formation: Implications for the Cenozoic Evolution of the Western Andes of Ecuador." *Minerals* 10, no. 10 (2020): 929. Accessed July 16, 2025. https://doi.org/10.3390/min10100929.

Verissimo Lobo, Victor Tozatto, Ronald Wbeimar Pacheco Ortiz, Vinicius Ottonio O Gonçalves, João Cajaiba, and Vinicius Kartnaller. "Kinetic Modeling of Maleic Acid Isomerization to

Fumaric Acid Catalyzed by Thiourea Determined by Attenuated Total Reflectance Fourier-Transform Infrared Spectroscopy." *Organic Process Research & Development* 24, no. 6 (2020): 988-96. Accessed July 20, 2025. https://doi.org/10.1021/acs.oprd.9b00487.

Verma, Gaurav. "Characterization Techniques." *Nanostructures*, 2023, 97-141. Accessed July 12, 2025. https://doi.org/10.1016/b978-0-12-820048-3.00011-5.

Villares, Fabián, Arturo Eguez, and Ernesto Yanez. "Petrographic and Geochemical Characterization of the Triassic and Jurassic Magmatic and Volcanic Rocks of Southeastern Ecuador." *EGU General Assembly Conference Abstracts*, 2014, 13614. Accessed July 16, 2025. https://ui.adsabs.harvard.edu/abs/2014EGUGA..1613614V.

Wilbert, Johannes. "The Thread of Life: Symbolism of Miniature Art from Ecuador." *Studies in Pre-Columbian Art and Archaeology*, no. 12 (1974): 1-112. http://www.jstor.org/stable/41263423.

Witt, C., J.Y Reynaud, D. Barba, et al. "From Accretion to Forearc Basin Initiation: The Case of SW Ecuador, Northern Andes." *Sedimentary Geology* 379 (January 2019): 138-57. Accessed July 16, 2025. https://doi.org/10.1016/j.sedgeo.2018.11.009.

Wright, Hedley G. "The Use of Epoxy Resins in the Preparation of Petrographic Thin Sections." *Mineralogical Magazine and Journal of the Mineralogical Society* 33, no. 265 (1964): 931-33. Accessed July 12, 2025. https://doi.org/10.1180/minmag.1964.033.265.11.

Wu, Haoyu, Mingyue He, Shaokun Wu, Mei Yang, and Xi Liu. "Near-Infrared Spectroscopy Study of OH Stretching Modes in Pyrophyllite and Talc." *Crystals* 12, no. 12 (2022): 1759. Accessed July 16, 2025. https://doi.org/10.3390/cryst12121759.

Xu, Shilong, Quanli Chen, Yan Li, and Xianyu Liu. "Blackish Green Omphacite Jade from Guatemala." *Gems & Geology* 59 (Fall 2023). Accessed July 16, 2025. https://www.gia.edu/gems-gemology/fall-2023-gemnews-blackish-green-omphacite-jade.

Yang, Wei, Sheng He, Ao Su, et al. "Paleo-Temperature and -Pressure Characteristics of Fluid Inclusions in Composite Veins of the Doushantuo Shale (Yichang Area, South China): Implications for the Preservation and Enrichment of Shale Gas." *Energy & Fuels* 35, no. 5 (2021): 4091-105. Accessed July 20, 2025. https://doi.org/10.1021/acs.energyfuels.1c00040.

Yang, Zhentao, Mingyue He, Shaokun Wu, Mei Yang, and Bijie Peng. "Near-Infrared Spectroscopic Study of Biotite?Phlogopite (Mg# = 30~99): OH-Stretching Modes and Mg# Content Prediction Equation." *Crystals* 14, no. 4 (2024): 336. Accessed July 16, 2025. https://doi.org/10.3390/cryst14040336.

Yardley, Bruce W.D. *An Introduction to Metamorphic Petrology*. Longman Scientific & Technical, 1989. Accessed July 23, 2025.

Zhao, H. X., Q. H. Li, S. Liu, Y. Q. Hu, and F. X. Gan. "Nondestructive Analysis of Jade Artifacts from the Cemetery of the Ying State in Henan Province, China Using Confocal Raman Microspectroscopy and Portable X?ray Fluorescence Spectroscopy." *Journal of Raman Spectroscopy* 45, no. 2 (2014): 173-78. Accessed July 12, 2025. https://doi.org/10.1002/jrs.4435.

Zumdahl, Steven S., Susan A. Zumdahl, and Donald J. DeCoste. *Chemistry*. 10th ed. Cengage, 2017.

APPENDICES

Appendix A - Code

A custom Python program was developed to streamline the visualization and analysis of the collected FT-IR spectral data.

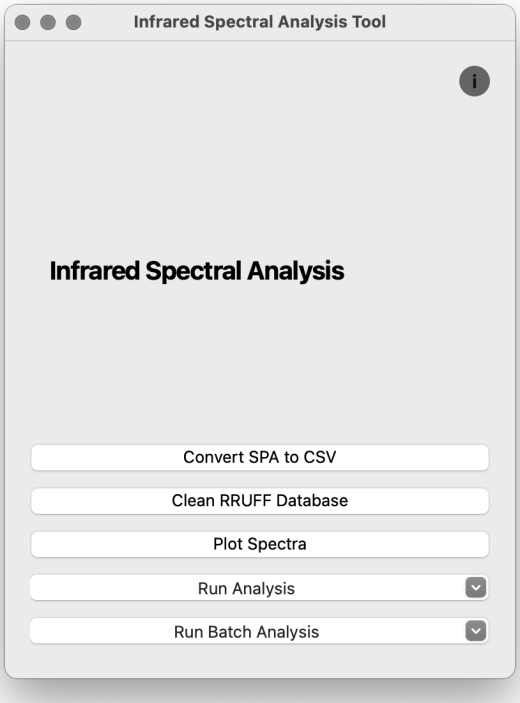

Figure A: Custom GUI interface

The source code for this project is available on GitHub at the following repository: https://github.com/jungkz/IR-Spectral-Analysis-GUI

Appendix B - Petrographic Photographs

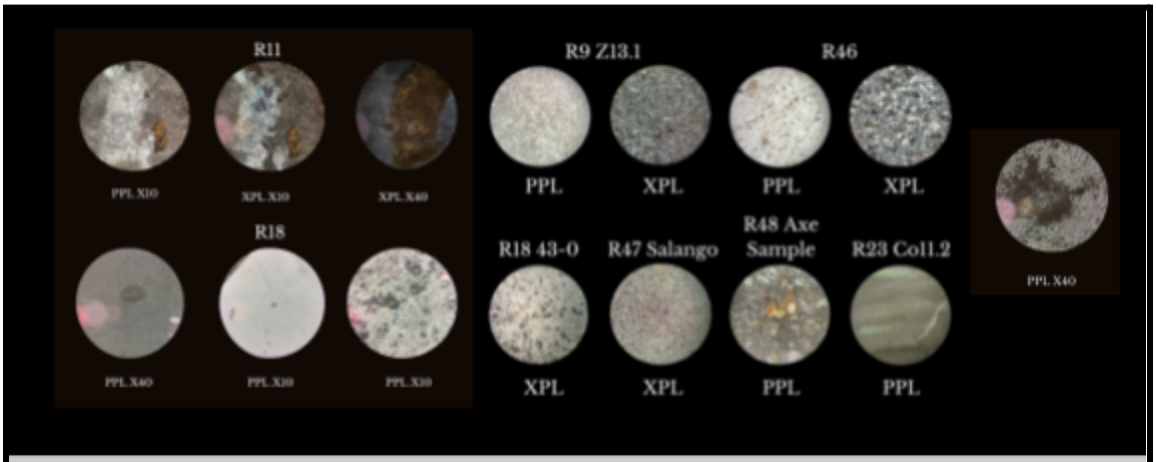

Figure B1: Petrographies from epoxy slides in polarized light and cross polarized light at different magnifications

Appendix C - FT-IR-ATR Spectra

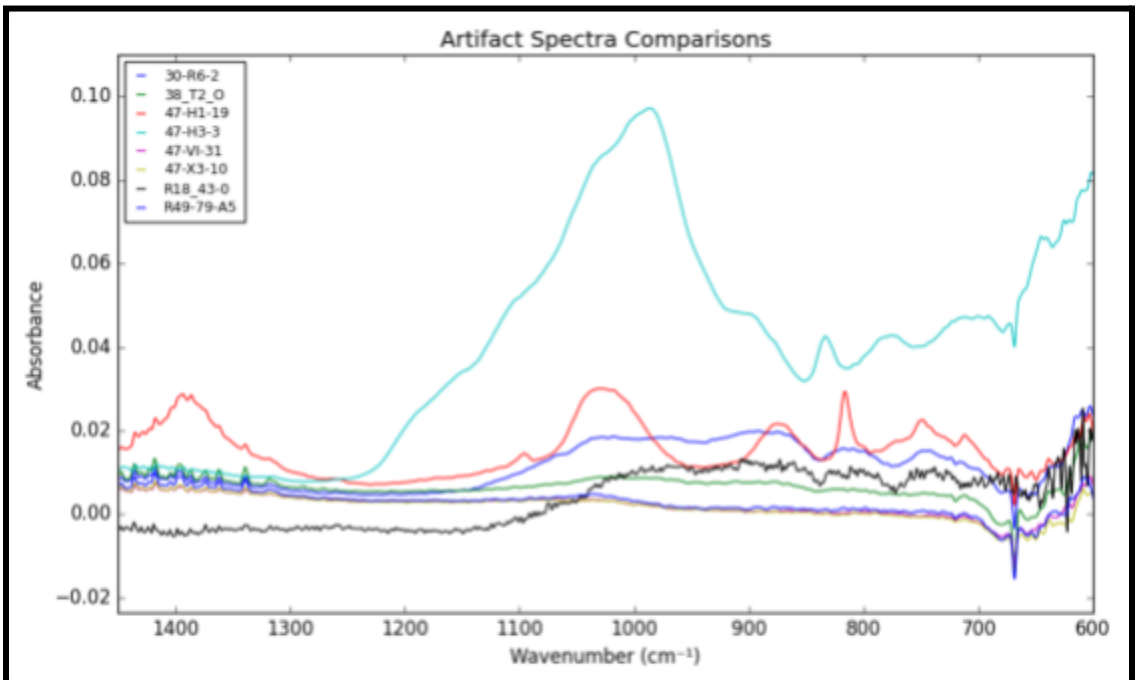

Figure C1: all artifacts' spectra overlayed

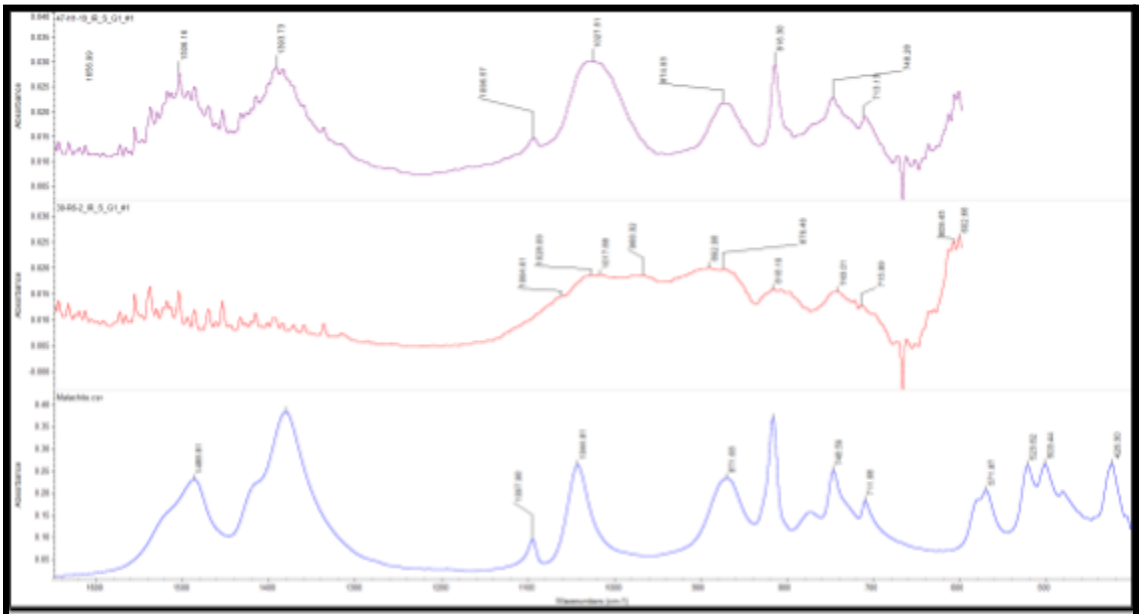

Figure C2: 47-H1-19 and 30-R6-2 spectra compared to malachite spectra

Appendix D - Visualizations of Statistical Analysis

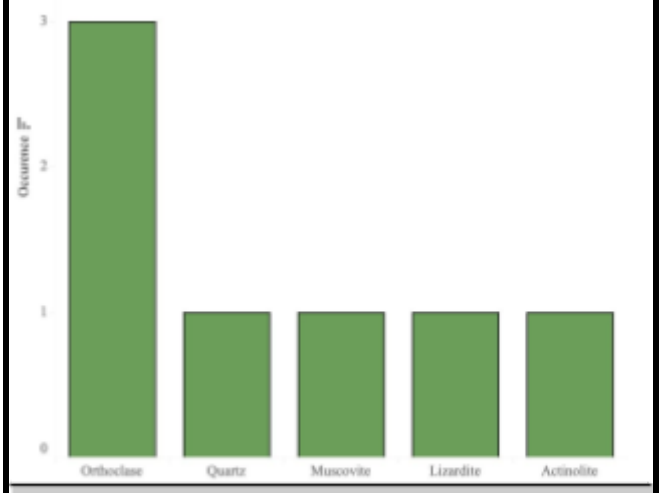

Figure D1: A Spearman's rank correlation analysis was used on accepted and collected FTIR spectra of the rock samples to identify their chemical composition. The occurrence of the most correlated identity for each sample is seen above (n = 7).

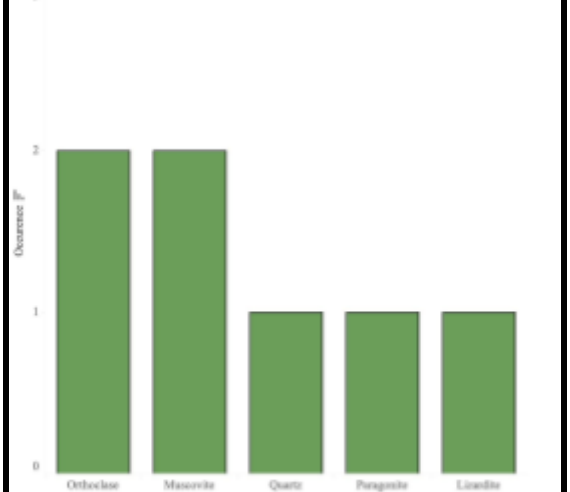

Figure D2: A Pearson's correlation analysis was used on accepted and collected FTIR spectra of the collected rock samples to identify their chemical composition. The occurrence of the most correlated identity for each sample is seen above (n = 7).

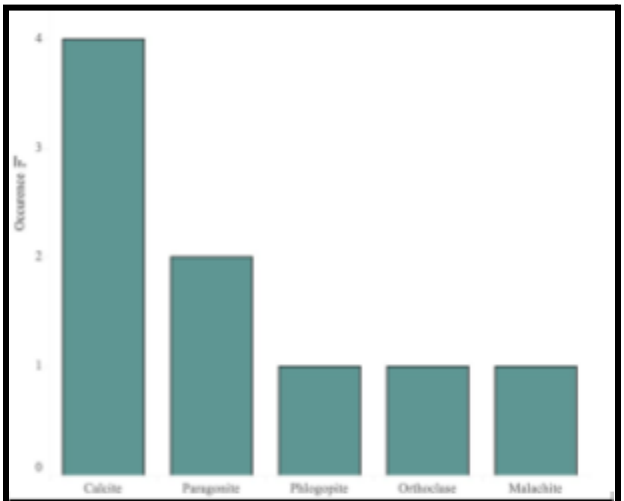

Figure D3: A Spearman's rank correlation analysis was used on accepted and collected FTIR spectra of artifacts to identify their chemical composition. The occurrence of the most correlated identity for each sample is seen above (n = 9).

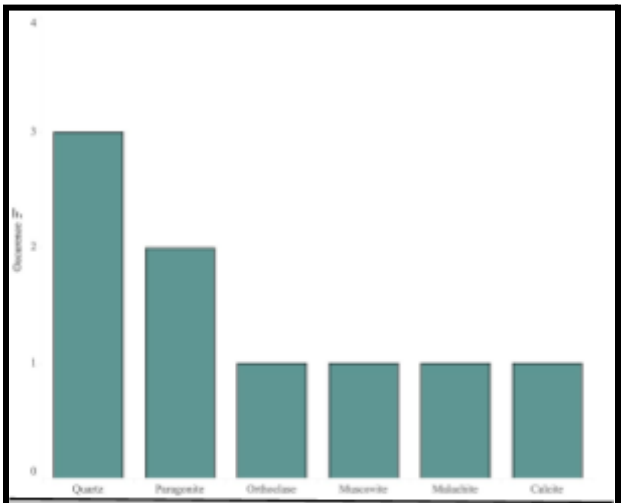

Figure D4: A Pearson's correlation analysis was used on accepted and collected FTIR spectra of artifacts to identify their chemical composition. The occurrence of the most correlated identity for each sample is seen above (n = 9).